Orbital and spin magnetism in US - comparison with USe and UTe

2001 J. Phys.: Condens. Matter 13 9677

(http://iopscience.iop.org/0953-8984/13/43/301)

INSTITUTE OF PHYSICS PUBLISHING JOURNAL OF PHYSICS: CONDENSED MATTER

J. Phys.: Condens. Matter **13** (2001) 9677–9690 PII: S0953-8984(01)25869-X

Orbital and spin magnetism in US—comparison with USe and UTe

N Kernavanois[1], P Dalmas de Réotier[1], A Yaouanc[1], J-P Sanchez[1], V Honkimäki[2], T Tschentscher[2,3], J McCarthy[2] and O Vogt[4]

[1] Commissariat à l'Energie Atomique, Département de Recherche Fondamentale sur la Matière Condensée, F-38054 Grenoble Cédex 9, France
[2] European Synchrotron Radiation Facility, BP 220, F-38043 Grenoble Cédex, France
[3] Hamburger Synchrotronstrahlungslabor HASYLAB at Deutsches Elektronen-Synchrotron DESY, Notkestrasse 85, D-22607 Hamburg, Germany
[4] Eidgnössische Technische Hochschule Zürich-Hönggerberg, Laboratorium für Festkörperphysik, CH-8093 Zürich, Switzerland

Received 18 June 2001, in final form 4 September 2001
Published 12 October 2001
Online at stacks.iop.org/JPhysCM/13/9677

Abstract

We report the results of two experiments performed on uranium monosulphide: measuring the magnetic Compton scattering (MCS) and x-ray magnetic circular dichroism (XMCD) at the $M_{4,5}$ uranium absorption edges. From the MCS experiment we get the spin moment of both the localized (5f electrons) and the diffuse (mainly 6d electrons) contributions. Combining these results with bulk magnetization and published neutron diffraction data, we can separate the orbital and spin contributions to the localized and diffuse moments. Using the XMCD measurements, we deduce the expectation value of the magnetic dipole operator. We finally compare our results on US with published measurements made on USe and UTe.

1. Introduction

In recent years, the study of uranium compounds has attracted much interest because of the variety of properties that these materials exhibit at low temperature. The spin–orbit interaction energy is of appreciable strength compared to the crystal-electric-field energy, and the itinerant or localized character of the 5f electrons depends on their hybridization with the conduction electrons or with the ligand valence states [1, 2]. Since a number of uranium intermetallics order magnetically, one important question is that of whether the magnetism is best described within a localized or an itinerant picture. As discussed for many instances, this central question can be addressed on the basis of the deviation of the orbital-to-spin ratio of the 5f moment compared to the prediction given for the ground state by the intermediate-coupling scheme [2]. Therefore it is important to separate experimentally the 5f orbital and spin contributions to the magnetization density in uranium compounds. Knowledge of these contributions underlies a

crucial test for theoretical methods of calculating these quantities [3–6]. In addition, it is of interest to determine whether the conduction electrons have weak orbital moments [7].

US belongs to the class of the uranium monochalcogenides that crystallize in the NaCl structure and it orders ferromagnetically at $T_C \simeq 177$ K (see table 1) [1]. Although thoroughly studied, the magnetism in US, classified as an itinerant ferromagnet, is not fully understood and remains a subject of current interest. US presents a bulk magnetization of 1.55(2) μ_B/f.u. at saturation [1] and a huge magnetocrystalline anisotropy at low temperature with the uranium moments pointing along the [111] easy direction [2]. From the slightly larger value $\mu(5f) = 1.70(3)\ \mu_B$ for the ordered 5f moment measured by means of polarized neutron diffraction [2, 11], it was concluded that the difference $\mu_{diff} = -0.15(4)\ \mu_B$ is essentially due to the diffuse U 6d conduction electrons which are polarized antiparallel to $\mu(5f)$ [1]. This antiparallel coupling was confirmed by spin-polarized photoemission experiments [12, 13] and deduced from magneto-optical measurements [14].

Table 1. Material parameters for the uranium monochalcogenides: lattice parameter a, Curie temperature T_C, bulk magnetic moment at saturation μ_{sat} [8] and 5f magnetic moment $\mu(5f)$ deduced from neutron diffraction experiments [9, 10]. The moments are given per uranium atom.

Compound	a (Å)	T_C (K)	μ_{sat} (μ_B)	$\mu(5f)$ (μ_B)
US	5.489	177	1.55(2)	1.70(3)
USe	5.740	160	1.81(5)	2.0(1)
UTe	6.155	104	1.91(5)	2.25(5)

The magnetic moment carried by the chalcogen atoms is generally considered negligibly small: the magnetization distribution deduced from magnetic neutron scattering data shows that the S moment is less than 0.02 μ_B [11]. It should however be noted that the S 3p bands have a small exchange splitting which is induced by the U moment [3]. Recently, a surprisingly large XMCD signal was observed at the sulphur K edge in US [15]. A similar huge enhancement was observed in resonant x-ray magnetic scattering experiments at the K edge of non-magnetic elements Ga and As in UGa_3 and UAs respectively [16]. To date there has been no definitive interpretation of these measurements; however, it is clear that the amplitude of the signals does not arise from large S or Ga and As moments [17].

Until recently, the study of the scattering vector dependence of the magnetic form factor, which can be accurately measured using polarized neutron diffraction, was the only technique suited to separating the orbital and spin contributions to the magnetization distribution in uranium compounds [1]. The information provided concerns essentially the U 5f moment owing to the rapid fall-off of the U 6d contribution to the form factor at small scattering vectors. The essential result is that the U orbital moment is much larger and antiparallel to the spin component in contrast to the situation encountered in 3d transition metals. This was confirmed by band-structure calculations, although the orbital moment was generally underestimated [3–5]. The actual values of the orbital and spin contributions to the U moment extracted from the fitting of the magnetic form factor depend somehow on the electron configuration assumed for the 5f shell. For US, Reim and Schoenes [14] concluded that the 5f occupation is 2.9, i.e. close to the U^{3+} configuration ($5f^3$), to be compared to the value of 2.54 estimated from band-structure calculations [3].

The experimental situation received a dramatic impulse with the advent of third-generation synchrotron sources whose high intensity allows one to explore the orbital and spin magnetization distributions using circularly polarized x-rays. Among the new emerging techniques, that based on x-ray magnetic circular dichroism (XMCD) with the aid of sum rules is well suited for determining the orbital and spin moments of a given electronic shell of a specific element.

Magnetic Compton scattering (MCS) measurement, which is also a relatively new technique, is solely sensitive to the total spin magnetization of the sample under study. The two techniques (see reference [18] for an introduction), which are complementary, both require the presence of a net magnetization, i.e. they are generally restricted to ferromagnets or ferrimagnets although experiments on paramagnets or even antiferromagnets are feasible if the magnetic polarization induced by the external field is sufficient.

In this paper, we first report results of MCS and XMCD measurements performed on US. In a second step, we combine our results with previous ones, in order to determine the different magnetic contributions. Finally, we discuss, in terms of the hybridization, their evolution in the uranium monochalcogenide series (US, USe, UTe).

We used the same US single crystal for the MCS and XMCD experiments. It was grown by mineralization at the Eidgnössische Technische Hochschule Zürich. Its dimensions are $\sim 6 \times 3$ mm^2 and its thickness is 2 mm.

We note that a first XMCD experiment was performed a few years ago on US by Collins *et al* [19]. As these authors used a second-generation synchrotron radiation source, the photon flux and the degree of circular polarization of the beam were lower compared to our case, giving rise to relatively large error bars in their results.

2. X-ray magnetic Compton scattering of US

The technique of x-ray MCS measurement is only sensitive to the spin magnetization. This peculiarity was first observed experimentally [20] and subsequently supported theoretically [21, 22]. Furthermore, different series of experiments demonstrated that this now established technique provides site-specific or even shell-specific information if the corresponding different electron shell momentum distributions are sufficiently different in shape.

2.1. Compton scattering cross-section

Compton scattering is an incoherent process which involves inelastic scattering of photons by electrons. The scattering cross-section for polarized photons scattered by a single free stationary electron was first given a long time ago within the impulse approximation, i.e. when the recoil energy of the ejected electron is sufficiently high compared with its binding energy [23]. The electron in the final state can then be treated as a plane wave. This approximation is valid in our case. It is written as

$$\frac{\mathrm{d}\sigma}{\mathrm{d}\Omega} = \frac{r_0^2}{2}\left(\frac{\omega_2}{\omega_1}\right)^2 \left[\left(\frac{\omega_1}{\omega_2} + \frac{\omega_2}{\omega_1} - (1 - P_l)\sin^2\theta\right) - P_c(1 - \cos\theta)\hbar\frac{\boldsymbol{\sigma}\cdot(\boldsymbol{k}_1\cos\theta + \boldsymbol{k}_2)}{mc}\right]. \tag{1}$$

ω_1 (ω_2) and $\boldsymbol{k}_1$ ($\boldsymbol{k}_2$) are respectively the energy and wave vector of the incident (scattered) photons; θ is the scattering angle. $r_0 = 2.8179 \times 10^{-15}$ m is the classical electron radius, m the electron mass, $\hbar$ the normalized Planck constant and c the velocity of light. P_l and P_c are the linear (relative to axes defined as the normal to the scattering plane and the axis perpendicular to it, in the scattering plane) and circular Stokes polarization factors for the incident photon flux, respectively, and $\boldsymbol{\sigma}$ is a unit vector indicating the direction of the spin. This expression is written for the case where the initial photon and electron polarizations are determined. It consists of a spin-independent term, called the charge term, plus a term which is linearly dependent on the initial electron spin, the magnetic term. Since these calculations have been performed for a stationary electron, this expression is strictly valid only for $p_z = 0$, where p_z is the projection of the electron momentum along the scattering vector $\boldsymbol{K} = \boldsymbol{k}_1 - \boldsymbol{k}_2$.

Considering Compton scattering against bound electron states, it has been shown with a fully relativistic treatment that the charge and magnetic cross-sections have different dependences on p_z [24]. In the momentum region comprising the width of a typical Compton profile (−20 atomic units (au) to +20 au) (1 au = 1.99×10^{-24} m kg s^{-1}), they are approximately linear in p_z with slopes that are only slightly different. This means that once the charge cross-section p_z-dependence has been accounted for, the magnetic cross-section dependence only constitutes a very small additional correction and the simple folding of the profile around $p_z = 0$ eliminates the need to include it.

For the p_z-dependence of the charge cross-section, we use the approximate relativistic treatment of the differential cross-section given by Ribberfors [25]:

$$\frac{\mathrm{d}^2\sigma}{\mathrm{d}\Omega\,\mathrm{d}\omega_2} = \frac{r_0^2}{2}\frac{m^2c^2}{\hbar K E}\frac{\omega_2}{\omega_1}\chi J_c(p_z) \tag{2}$$

where χ is defined by

$$\chi = \frac{R}{R'} + \frac{R'}{R} + 2m^2c^4\left(\frac{1}{R} - \frac{1}{R'}\right) + m^4c^8\left(\frac{1}{R} - \frac{1}{R'}\right)^2 \tag{3}$$

with

$$R = \frac{\omega_1\omega_2(1-\cos\theta)}{\hbar^2K^2c^2}(E\omega_1 + E\omega_2 + \omega_1^2 - \omega_1\omega_2\cos\theta) \tag{4}$$

$$R' = \frac{\omega_1\omega_2(1-\cos\theta)}{\hbar^2K^2c^2}(E\omega_1 + E\omega_2 - \omega_2^2 + \omega_1\omega_2\cos\theta). \tag{5}$$

The momentum transfer is

$$\hbar K = \hbar|\boldsymbol{k}_1 - \boldsymbol{k}_2| = \sqrt{\omega_1^2 + \omega_2^2 - 2\omega_1\omega_2\cos\theta}/c$$

and the total energy of the electron is $E \approx \sqrt{m^2c^4 + p_z^2c^2}$ with the approximation $p^2 \approx p_z^2$. In the relativistic framework, p_z is [26]

$$p_z = \frac{\hbar K}{2} - \frac{\omega_1 - \omega_2}{2c}\sqrt{1 + \frac{2m^2c^4}{\omega_1\omega_2(1-\cos\theta)}}. \tag{6}$$

In equation (2), $J_c(p_z)$ is the charge Compton profile (CCP), i.e. the projection of the electron momentum density, $n(\boldsymbol{p})$, along the scattering vector. It is normalized following the relation $\int_{-\infty}^{+\infty} J_c(p_z)\,\mathrm{d}p_z = Z_{\mathrm{eff}}$, where Z_{eff} is the number of electrons involved in the scattering process.

The magnetic Compton profile (MCP) $J_{\mathrm{mag}}(p_z)$ is the difference of the projections of the electron momentum densities for spin up and spin down. To obtain $J_{\mathrm{mag}}(p_z)$ from the data, we need to express it in terms of the measured cross-section. We propose the following extension of equation (2):

$$\left(\frac{\mathrm{d}^2\sigma}{\mathrm{d}\Omega\,\mathrm{d}\omega_2}\right) = \frac{r_0^2}{2}\frac{m^2c^2}{\hbar K E}\frac{\omega_2}{\omega_1}\chi[J_c(p_z) + \alpha J_{\mathrm{mag}}(p_z)]. \tag{7}$$

This form, where α is p_z-independent, follows from our basic approximation (see above, equation (2)). Explicitly we take α as the ratio of the charge and magnetic terms in equation (1):

$$\alpha = -P_c(1-\cos\theta)\hbar\boldsymbol{\sigma}\cdot(\boldsymbol{k}_1\cos\theta + \boldsymbol{k}_2)\Big/mc\left(\frac{\omega_1}{\omega_2} + \frac{\omega_2}{\omega_1} - (1-P_l)\sin^2\theta\right).$$

As we are no longer dealing with a single electron, $\boldsymbol{\sigma}$ is now redefined as a unit vector parallel to the magnetization. $J_{\mathrm{mag}}(p_z)$ can be obtained by recording two sets of spectra with opposite values of P_c or $\boldsymbol{\sigma}$. $|\alpha|$ is typically $\lesssim 1$ and $|\alpha J_{\mathrm{mag}}(p_z)/J_c(p_z)| \sim 10^{-2}$ since the number of unpaired electrons is small relative to Z_{eff}.

The total spin moment of the compound under study is given, in units of the Bohr magneton, by the area of the profile $\int_{-\infty}^{+\infty} J_{\mathrm{mag}}(p_z)\ \mathrm{d}p_z$. The magnetic spin contributions of the different electronic shells involved in the magnetism are obtained by fitting theoretical profiles to $J_{\mathrm{mag}}(p_z)$.

2.2. Data analysis

In order to determine the experimental CCP, six corrections have been applied to the raw data. We list them below. Details can be found elsewhere [27].

The cross-section has been corrected for the energy dependence of the detector efficiency which is determined by the absorption of the germanium crystal.

We need to consider the parasitic CCP induced by the Kapton windows of the refrigerator. As usual, this has been evaluated with a measurement with no sample in the refrigerator. The fraction of signal arising from Kapton is ∼9.9% of the total.

To compare the measured CCP to the theoretical one, one has to account for the experimental resolution function. It can be measured from the spread in energy of the elastically scattered photons or the fluorescence lines. It is a slightly asymmetric Gaussian function due to the incomplete charge collection of the Ge crystal of the detector. It can be mimicked by a convolution product of a Gaussian with a right-angle-triangle-shaped function, the tail of which is on the low-energy side. The parameters of this function were fitted. The full width at half-maximum of the Gaussian is, in momentum units, 0.54 au and the area of the triangle function is only 1.8% of the area of the Gaussian. In order (i) to ensure that the CCP obtained from our measured cross-section is symmetrical around $p_z = 0$, as it has to be, and (ii) to be able to work on the folded magnetic profile as required to compensate for the different p_z-dependences of the charge and magnetic cross-sections, we prefer to correct the weak asymmetry of the resolution function at this stage. Therefore we have convoluted the experimental data with the triangle function and subtracted the result from the original data. The area of the subtracted data is therefore 1.8% of the total area of the original experimental data.

We have considered the effect of multiple scattering [28]. When integrated over energy, the proportion of the single-, double- and triple-scattering events amounts to 86%, 12% and 2%, respectively.

We have also corrected the cross-section for the absorption in the US sample itself.

Finally, we have determined the residual background originating from non-Compton scattering events. In the restricted region of interest, say $|p_z| < 20$ au, it is almost linear in p_z and its area represents 4.2% of the CCP area.

We emphasize that the corrections performed on the raw data leave the shape of the MCP essentially unaffected. They only influence the normalization coefficient, i.e. the total spin moment. This can be easily understood, as the corrections apply in essentially similar ways for the two sets of data recorded with the two opposite polarizations.

2.3. Experimental procedure

The measurements were performed at the end-station of beamline ID15A of the European Synchrotron Radiation Facility (ESRF), Grenoble, France, where the best conditions for MCS experiments can be achieved [29].

We used a standard backscattering geometry which is displayed in figure 1.

The energy of the incident photons was $\omega_1 = 104.36$ keV, below the absorption K-edge energy of uranium (115.6 keV). At this energy, which is about twice that used in earlier

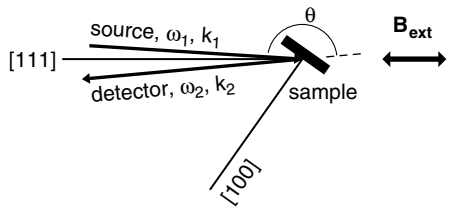

Figure 1. The schematic scattering geometry of the Compton experiment. The scattering angle is $\theta = 171.2^\circ$. The scattering vector $\boldsymbol{K}$ corresponding to photons scattered by electrons at rest is parallel to the [111] crystal axis. The angle between the incident beam and [111] is 3.7°. An external magnetic field, $\boldsymbol{B}_{\rm ext}$, of magnitude 0.9 T is applied alternately parallel and antiparallel to the [111] direction. The data were recorded for a duration of 50 s after a sleeping time of 5 s following the field reversal.

experiments [30, 31], the absorption in the sample is decreased, the magnetic contribution increased and the momentum resolution improved.

We used a closed-cycle refrigerator and the magnetic field of 0.9 T was applied along the [111] crystal axis which is the easy axis. Due to the huge magnetic anisotropy of US at low temperature [2], the data were recorded at 160 K (still below $T_C = 177$ K) to minimize the magnetic torque acting on the sample while the magnet rotates. At this temperature the magnetic anisotropy of US is reduced as compared to that at low temperatures and the magnetization is still sizable [2]. Under these conditions we measured a bulk magnetic moment $\mu_{\rm bulk} = 1.08(5)\ \mu_B$/f.u. on our crystal. To simplify comparisons, we renormalized all the values for the different moments given in this paper to saturation at low temperature, using the bulk magnetization temperature dependence measured for our sample as reference.

In order to experimentally determine P_l and P_c, an auxiliary measurement was performed on metallic Fe with the same experimental set-up and the same geometry. We used the result $\int_{-\infty}^{+\infty} J_{\rm mag}(p_z)\,{\rm d}p_z = 2.12$ for Fe [32].

The flipping ratio defined as the ratio between the difference and sum of counts in the Compton peak region for the two orientations of the field was $-0.218(5)\%$ for US and $1.97(2)\%$ for Fe.

2.4. Results

In figure 2(a), we compare the CCP with the calculated one convoluted with the Gaussian resolution function. The theoretical atomic profiles describe accurately the inner-shell momentum densities for $|p_z| > 2$ au. Conduction electrons, which are at low momentum density, are not well accounted for in this model due to solid-state effects. The nice agreement between the corrected data and the calculated line for $|p_z| > 2$ au in figure 2(a) shows that the different corrections have been properly performed.

The MCP of US is shown in figure 2(b). It is negative, reflecting that the spin moment of US is antiparallel to $\boldsymbol{B}_{\rm ext}$. This is expected, as the main contribution to the bulk magnetic moment of US is the 5f orbital moment which is therefore parallel to $\boldsymbol{B}_{\rm ext}$. Also, the dominant contribution to the MCP arises from the uranium 5f electrons, whose spin moment is antiparallel to the 5f orbital moment, following Hund's rule.

The total area of the MCP gives the total spin moment of US, $\mu_S = -1.33(9)\ \mu_B$. The error bar given here corresponds to statistical errors and uncertainties introduced by the normalization to saturation magnetization at low temperature. The MCP is then analysed in the region with $p_z > 2$. Among the electronic shells liable to be magnetized, the only one

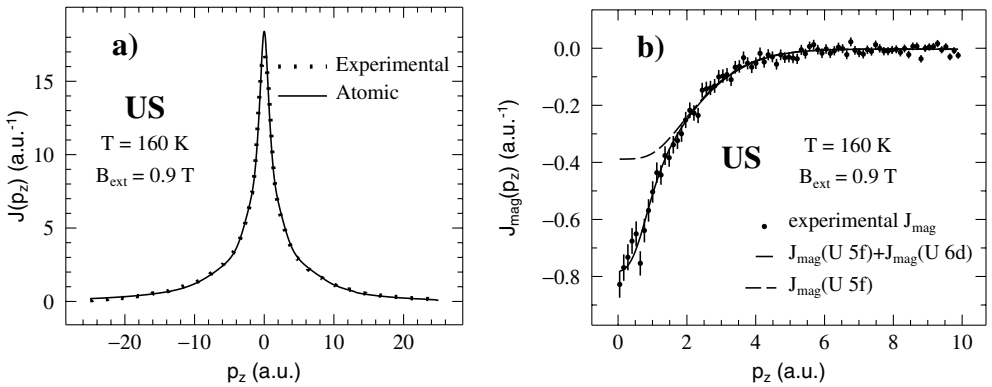

Figure 2. (a) Comparison between the measured and calculated (from reference [33]) charge Compton profiles of US. (b) The magnetic Compton profile of US (filled circles) and the fit (solid line) obtained from the 5f and 6d free-atom calculated profiles of U convoluted with the experimental resolution function. The dashed line is the contribution of the 5f electrons of uranium.

with sizable momentum density above 2 au is the 5f shell (figure 3). Therefore we fit the data with $p_z > 2$ au to the 5f theoretical atomic profile (convoluted with the resolution function). We deduce the 5f spin moment $\mu_S(5f) = -0.97(7)\ \mu_B$. The remaining part of the MCP characterizes the diffuse spin moment arising from other electronic shells. It turns out that, as shown in figure 2(b), the diffuse contribution to the MCP is well fitted by the U 6d atomic theoretical profile and we find $\mu_S(\text{diff}) = -0.36(3)\ \mu_B$. We note that the S 3p shell has a very similar profile to the U 6d one (figure 3).

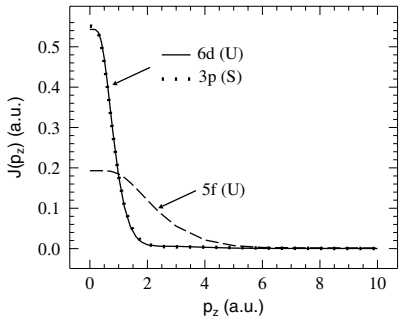

Figure 3. Different normalized free-atom Compton profiles [33] of selected electrons of US.

3. X-ray magnetic circular dichroism at the $M_{4,5}$ edges of US

3.1. Background

The XMCD technique has opened up the possibility of probing the magnetic moment of a given chemical element with electronic shell selectivity. It consists of measuring, at energies in the vicinity of an absorption edge, the difference in absorption of x-rays with different handedness of circular polarization. For probing the 5f shell of uranium, the $M_{4,5}$ edges located at 3.73 and 3.55 keV are suitable, as they involve the electronic $3d_{3/2,5/2} \longrightarrow 5f$ transitions. With the help of the sum rules [34, 35], this new magnetometry tool allows one

to measure $\langle L_z\rangle/n_h$ and $\langle L_z\rangle/\langle S_z^e\rangle$ with $\langle S_z^e\rangle \equiv \langle S_z\rangle + 3\langle T_z\rangle$ where $\langle L_z\rangle$, $\langle S_z\rangle$ and $\langle T_z\rangle$ are the expectation values of the z-projections of respectively the orbital angular momentum, the spin angular momentum and the magnetic dipole operators of the 5f shell and n_h is the number of holes in this shell.

One of the assumptions made in the derivation of the sum rules is that the U $3d_{3/2,5/2}$ core levels are characterized by a large spin–orbit splitting, much larger than other relevant interactions (e.g. the intra-atomic 3d–5f exchange interaction). This condition is clearly fulfilled for uranium.

We will use the first sum rule [34] to derive $\langle L_z\rangle$. The orbital moment of the U 5f shell is given by $\mu_L(5f) \equiv -\langle L_z\rangle\,\mu_B$. The use of the second sum rule [35] is more tricky because of the presence of both $\langle S_z\rangle$ and $\langle T_z\rangle$. Usually, together with the second sum rule, one uses a model estimate for $\langle T_z\rangle$ and thereafter deduces $\langle S_z\rangle$ [36]. Here we will use the experimental MCS value for $\langle S_z\rangle$ to deduce a value for $\langle T_z\rangle$.

3.2. Experimental procedure

XMCD measurements were carried out at the ESRF beamline ID12A, which is dedicated to polarization-dependent x-ray absorption studies [37, 38]. The source is the helical undulator Helios-II which provides high flux, high circular polarization rate (about 0.97) and tunable helicity of the incoming beam. The monochromator was equipped with a pair of Si(111) crystals. Due to the monochromator set-up, the computed degree of circular polarization of the beam at the sample is dramatically reduced. It was estimated to be 0.35 and 0.45 respectively at the M_5 and M_4 edges [39].

The spectra were recorded at 160 K in the fluorescence-yield detection mode. Although the fluorescence is not strictly proportional to the absorption [19], this method gives reliable results for uranium compounds as far as the use of the sum rules is concerned [40]. The two spectra needed for the dichroism were recorded by flipping the direction of the applied magnetic field of 2 T produced by a superconducting cryomagnet (i.e. parallel and antiparallel to the direction of the incoming beam). This method is equivalent to switching the handedness of the circular polarization. For experimental reasons the easy magnetization axis [111] of US made a 45° angle with $\boldsymbol{B}_{\rm ext}$ in the plane defined by the directions [111] and [100]. The external field was applied along the direction of the x-ray beam (figure 4). A separate measurement of the total bulk magnetization of US under the same geometrical conditions leads to a moment of 0.97(5) μ_B. As for the MCS, the experimental values given in the following are renormalized to low-temperature saturation.

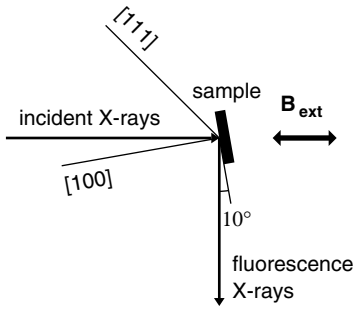

Figure 4. A schematic top view of the experiment

The fluorescence spectra have been corrected for self-absorption effects using a well established procedure [36,41] to give the absorption spectra. We note that, because the XMCD signal at the M_5 edge is much weaker than that at the M_4 edge, the self-absorption correction has a negligible influence on the size of the moments deduced from the two sum rules.

3.3. Estimation of the uncertainties

Our estimate of the uncertainties which takes into account both the transformation from fluorescence to absorption and the application of the sum rules, but not the intrinsic sum rule uncertainties, gives relative variations of 7% on $\langle L_z\rangle/3n_h$ and less than 1% on $\langle L_z\rangle/\langle S_z^e\rangle$. The smaller uncertainty in the ratio $\langle L_z\rangle/\langle S_z^e\rangle$ is easily understood, as the simultaneous use of the two sum rules means that the areas of the absorption white lines are not required because they cancel out in the ratio. From our results, we deduce that the data treatment has no real influence on the orbital-to-spin ratio ($\lesssim$1%). Considering the intrinsic approximation in the sum rules and the uncertainty introduced by the self-absorption correction and the use of these sum rules, we finally estimate an upper bound for the total uncertainties: 10% on $\langle L_z\rangle/3n_h$ and 4% on $\langle L_z\rangle/\langle S_z^e\rangle$.

3.4. Results

In figure 5 we present the fluorescence and difference spectra recorded for US. Figure 6 displays the absorption and dichroism spectra obtained from the fluorescence spectra of US. Whereas the shape of the dichroism spectrum at the M_4 edge more or less scales with the corresponding white line, the M_5 one has a peculiar structure. The extremum of the dichroic signal occurs at an energy lower than that of the maximum of the absorption. In addition, a positive structure is observed on the high-energy side of the extremum. This shape was already suggested by the work of Collins *et al* [19] on US. It was also observed for other uranium compounds and a qualitative interpretation for it has been given in reference [43]. The application of the sum rules yields $\langle L_z\rangle/3n_h = -0.079(13)$ and $\langle L_z\rangle/\langle S_z^e\rangle = -1.56(6)$. For the $\langle L_z\rangle/3n_h$ value, we have taken into account the uncertainty due to the renormalization to the saturation at low temperature. Comparing to reference [19] we find a value of $\langle L_z\rangle/3n_h$ that is somewhat lower ($\sim$20%) whereas that of $\langle L_z\rangle/\langle S_z^e\rangle$ is very similar.

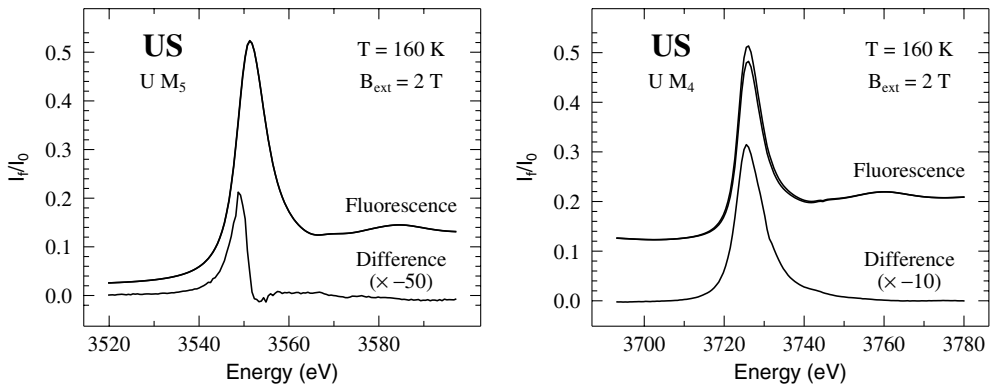

Figure 5. Fluorescence and difference spectra at the $M_{4,5}$ edges of uranium in US at 160 K and 2 T. For each edge we present the fluorescence spectra recorded for the two opposite directions of $\boldsymbol{B}_{\rm ext}$. The difference between the two spectra at the M_5 edge is almost invisible in the figure.

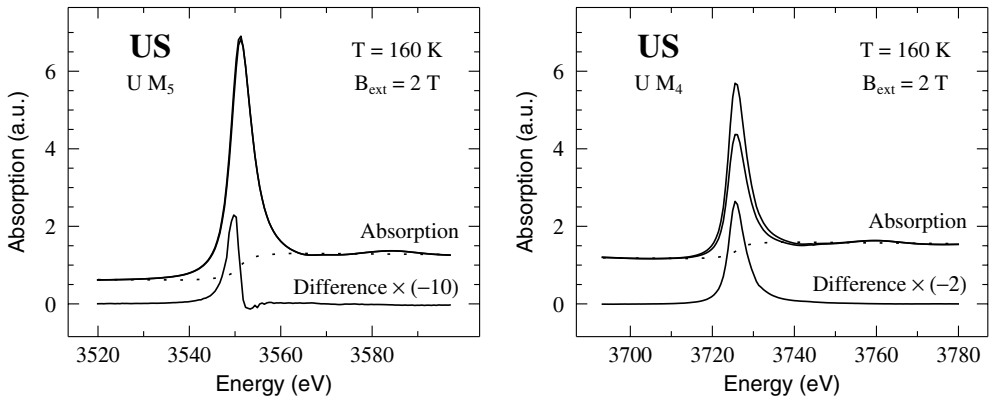

Figure 6. Absorption and dichroism spectra at the $M_{4,5}$ edges of uranium in US at 160 K and 2 T. The absorption spectra have been deduced from the fluorescence spectra which have been corrected for self-absorption and energy dependence of the circular polarization rate of the monochromatic beam. For each edge, the two absorption spectra correspond to the two opposite directions of $\boldsymbol{B}_{\text{ext}}$. The difference between the two spectra at the M_5 edge is almost invisible in the figure. The dotted line is the step-like function used for the background determination.

The determination of the orbital contribution to the 5f magnetic moment requires a value for n_h. It can be derived from band-structure calculations. Taking the 5f occupation number (namely 2.54) computed by Trygg *et al* [3], it follows that $n_h = 11.46$. Then the application of the first sum rule leads to $\langle L_z \rangle = -2.7(4)$. This means that the uranium ions carry a 5f orbital moment of $\mu_L(5f) = 2.7(4)\ \mu_B$ parallel to the applied field, as expected. We note that assuming a uranium valency of +3, i.e. $n_h = 11$, would not change the result significantly. Combining $\mu_L(5f)$ with the total 5f moment $\mu(5f) = 1.70(3)\ \mu_B$ obtained from neutron scattering [11], we get $\mu_S(5f) = -1.0(4)\ \mu_B$ in nice agreement (although less accurate) with the MCS result. This confirms the consistency of the data obtained by different techniques.

4. Orbital and spin magnetism in US; comparison with USe and UTe

The MCS results in combination with the total and 5f moments as determined by magnetization and neutron diffraction experiments allow for the separation of the spin and orbit contributions to the different magnetic moments in US. From the MCS saturated spin moment ($-1.33(9)\ \mu_B$) and the bulk magnetization value ($1.55(2)\ \mu_B$) we can deduce the total orbital magnetic moment of US as follows: $\mu_L = \mu - \mu_S = 2.88(9)\ \mu_B$. As $\mu_S(5f)$ and $\mu_S(\text{diff})$ are known from the MCS results and $\mu(5f)$ and $\mu(\text{diff})$ from the combined analysis of neutron and magnetization measurements, we obtain $\mu_L(5f) = \mu(5f) - \mu_S(5f) = 2.67(8)\ \mu_B$ and $\mu_L(\text{diff}) = \mu(\text{diff}) - \mu_S(\text{diff}) = 0.21(5)\ \mu_B$. The different contributions to the magnetic moments in US are summarized in table 2.

From the definition of $\langle S_z^e \rangle$, we can write

$$\langle T_z \rangle = \frac{\langle L_z \rangle}{3}\left(\frac{\langle S_z^e \rangle}{\langle L_z \rangle} - \frac{\langle S_z \rangle}{\langle L_z \rangle}\right). \tag{8}$$

The XMCD provides a precise estimate for the ratio $\langle L_z \rangle / \langle S_z^e \rangle$ ($-1.56(6)$). Taking this together with $\langle L_z \rangle = -\mu_L(5f)/\mu_B = -2.67(8)$ and $\langle S_z \rangle = -\mu_S(5f)/(2\mu_B) = 0.48(3)$ taken from table 2, we find $\langle T_z \rangle = 0.41(4)$.

Table 2. Different magnetic contributions for US, USe and UTe, in units of μ_B, deduced from MCS experiment values (analysis of Compton data recorded on USe and UTe in reference [31], this work for US) combined with magnetization and neutron scattering data (table 1). We do not make any hypothesis regarding the diffuse orbital moment and reasonable uncertainties have been added to the UTe results. The orbital-to-spin ratios for 5f electrons determined from the MCS (using the neutron value for the total 5f moment), neutrons [9, 45, 46] and calculations for free ions assuming an intermediate-coupling scheme [19, 44] are also indicated. The error bars on the neutron orbital-to-spin ratios for US and UTe have been determined by fitting the published data.

	US	USe	UTe
μ_L	2.88(9)	3.21(6)	3.25(7)
μ_S	−1.33(9)	−1.40(3)	−1.34(5)
μ(5f)	1.70(3)	2.0(1)	2.25(5)
μ_L(5f)	2.67(8)	3.1(1)	3.26(7)
μ_S(5f)	−0.97(7)	−1.09(2)	−1.01(5)
μ(diff)	−0.15(4)	−0.19(11)	−0.34(7)
μ_L(diff)	0.21(5)	0.12(11)	−0.01(9)
μ_S(diff)	−0.36(3)	−0.31(1)	−0.33(5)
$-\mu_L(5f)/\mu_S(5f)$:			
Compton	2.75(22)	2.84(11)	3.23(17)
Neutrons ($5f^3$)	2.4(3)	—	2.2(4)
Free ions ($5f^3$)	2.54	2.54	2.54
Free ions ($5f^2$)	3.36	3.36	3.36

The comparison of the experimental values of $\langle L_z\rangle$, $\langle S_z\rangle$ and $\langle T_z\rangle$ with those computed for two $5f^n$ ground-state configurations (table 3) indicates that both $\langle S_z\rangle$ and $\langle L_z\rangle$ lie close to the $5f^3$ configuration values, but this configuration is not confirmed by the value of $\langle T_z\rangle$. However, we note that (i) the theoretical value of $\langle T_z\rangle$ depends slightly on the parameters of the intermediate coupling: $\langle T_z\rangle = 0.31$ according to reference [19] and 0.33 according to reference [44] and (ii) the Hartree–Fock calculations for US [6] predict[1] $\langle T_z\rangle = 0.36$ with a 5f electron number of 2.88. This indicates a certain uncertainty for the theoretical values of the expectation values of the operators. The fact that, according to the values of $\langle S_z\rangle$ and $\langle L_z\rangle$, the electronic state of U in US is close to the $5f^3$ state is in agreement with a previous experimental result [14].

Table 3. The moments for the $5f^n$ atomic ground-state configurations calculated with the intermediate-coupling scheme using published data [44]. The moments have been rescaled by the same factor to reproduce the known total 5f moment, μ(5f). The calculated total moments before rescaling are denoted by $\mu(5f)^*$.

Configuration	$\langle L_z\rangle$	$\langle S_z\rangle$	$\langle T_z\rangle$	$\langle S_z^e\rangle$	$\langle L_z\rangle/\langle S_z^e\rangle$	μ(5f) (μ_B)	$\mu(5f)^*$ (μ_B)
U $5f^2$	−2.42	0.36	0.42	1.62	−1.49	1.70	3.30
U $5f^3$	−2.76	0.53	0.33	1.52	−1.82	1.70	3.43

Since we have established the different magnetic contributions in US, of particular interest here are the studies of Sakurai *et al* [30] and Hashimoto *et al* [31] performed on the ferromagnets UTe and USe, respectively. The values of the spin moments of the 5f and the so-called diffuse electrons for both UTe and USe have been determined by means of magnetic Compton scattering.

[1] In our convention the z-axis is oriented parallel to $\boldsymbol{B}_{\rm ext}$.

Using the same procedure as for US, we determine the different magnetic contributions of USe and UTe without restriction on the μ_L(diff) value, but using the data obtained from neutron scattering [9, 10, 45]. Thus, we are able to compare the magnetic moments of the chalcogenide UX series (X = S, Se, Te) and see the effects of the size of the chalcogenide element. We expect the degree of localization of the 5f electrons to increase with the atomic number of the chalcogenide element. The results are given in table 2. Examining that table, we first notice that μ(5f) increases in accordance with the saturated magnetization and the lattice parameter (see table 1). μ_L(5f) follows the same trend, while μ_S(5f) seems to be roughly constant. Moreover, we notice the parallel coupling of μ_S(5f) and μ_S(diff).

The most original feature arises from the non-vanishing orbital moment for the diffuse magnetic moment for the first two compounds. Although for USe the error bar is quite large compared with the absolute value, our data for US clearly indicate a finite value. This reflects a relatively strong spin–orbit coupling for the diffuse electrons. A similar orbital polarization of the 5d band was observed in several rare-earth compounds [7]. Furthermore, we note that μ_L(diff) decreases monotonically from US to UTe. Also, like μ_S(5f), μ_S(diff) does not vary significantly.

The ratio $-\mu_L(5f)/\mu_S(5f)$ estimated from MCS data can be compared to the one deduced from the fit of the neutron magnetic form factor and to the free-ion values calculated within the intermediate-coupling scheme. A rather good agreement within error bars is obtained between all of these values, assuming a U^{3+} valence state for US. Whereas the error bars include the MCP, neutron and theoretical values for US, this is not the case for USe and a large discrepancy is observed for UTe.

It is generally assumed for the uranium monochalcogenide series that the 5f electrons are localized with a $5f^3$ ground state in UTe whereas in US they should be hybridized, the situation for USe being intermediate. However, the experimental orbital-to-spin ratio for US shows that the 5f electrons are only weakly hybridized, since it is very close to the free-ion value. We would then anticipate $-\mu_L(5f)/\mu_S(5f)$ to be almost equal to the free-ion ratio for USe and UTe. This is not observed experimentally, in particular for UTe. Considering now the Compton results separately, we notice that throughout the UX series, the Compton values would indicate a $5f^3$ ground state with a weak hybridization for US, a $5f^2$ ground state for UTe and an intermediate configuration for USe. Within this picture, the Compton and neutron results for UTe are consistent, since the fit of the neutron data gives $-\mu_L(5f)/\mu_S(5f) = 2.6(5)$ under the hypothesis of a $5f^2$ configuration. The Compton and neutron ratios are still smaller than the free-ion $5f^2$ value. This would indicate that in fact the electronic configuration of U in UTe is not purely $5f^2$. Since the attribution of a $5f^2$ ground state for the 5f electrons in UTe is unconventional, more experiments are needed to support our conclusion; in particular, polarized neutron diffraction studies on USe seem not to have been performed.

A note of caution is in order concerning the information extracted from the magnetic Compton profile. The theoretical atomic profile for the 5f electrons is only used in a p_z-region in which its shape is thought to be reliable. However, this profile is normalized. Therefore, if the area for $p_z < 2$ au is very different from the atomic estimate, the profile for $p_z > 2$ au will be changed and then the 5f spin moment estimate will not be correct. For instance, if the area for $p_z < 2$ au was notably smaller than that given by the available theory, the absolute value of the 5f spin moment would be larger than that given in table 2. Clearly a theoretical study of the magnetic Compton profiles would be worthwhile. This remark points more generally to the limitations of the models currently available for the interpretation of MCS and XMCD data: these models are based on atomic physics, and subtle effects including electron delocalization and hybridization are not well accounted for. Our treatment of the XMCD data also neglects coherence effects which could modify the ratio between the dichroic signals [47].

5. Conclusions

MCS measurements have been performed on US at 160 K and 0.9 T and XMCD experiments at the $M_{4,5}$ edges of uranium at 160 K and 2 T. Combining the MCS results with the bulk magnetization and neutron scattering data, we separate the spin and orbital moments of the 5f shell and diffuse electrons. We find a non-zero orbital moment on the diffuse (mainly 6d) component, parallel to the field direction and therefore to the 5f orbital moment.

We can ascribe the diffuse moment measured by means of MCS to the 6d electrons on the grounds of neutron work, which concludes that there is a negligible moment on sulphur. Part of the diffuse moment that we observe could eventually arise from sulphur 3p electrons. This however would not change our main conclusion, which concerns the existence of an orbital component for the magnetic moment of the diffuse electrons.

The orbital and spin moments indicate a $5f^3$ atomic ground-state configuration of U in US, in agreement with previous experimental results.

Concerning the tendency in the chalcogenide series UX, we confirm the trend of localization of the U 5f electrons: the orbital magnetic moments increase with the lattice parameter while the spin contributions do not vary significantly.

Acknowledgment

A Rogalev is gratefully acknowledged for providing us with excellent working conditions at beamline ID12A of ESRF.

References

[1] *Handbook on the Physics and Chemistry of the Actinides* 1984 vol 1, ed A J Freeman and G H Lander (Amsterdam: North-Holland)
Handbook on the Physics and Chemistry of the Actinides 1985 vol 2, ed A J Freeman and G H Lander (Amsterdam: North-Holland)
Handbook on the Physics and Chemistry of the Actinides 1989 vol 5, ed A J Freeman and G H Lander (Amsterdam: North-Holland)
Lanthanides/Actinides (Handbook on the Physics and Chemistry of the Rare Earths vol 17) 1993 ed K A Gschneidner Jr, L Eyring, G H Lander and G R Choppin (Amsterdam: North-Holland)
[2] Lander G H, Brooks M S S, Lebech B, Brown P J, Vogt O and Mattenberger K 1991 *J. Appl. Phys.* **69** 4803
[3] Trygg J, Wills J M, Brooks M S S, Johansson B and Eriksson O 1995 *Phys. Rev.* B **52** 2496
[4] Severin L, Brooks M S S and Johansson B 1993 *Phys. Rev. Lett.* **71** 3214
[5] Kraft T, Oppeneer P M, Antonov V N and Eschrig H 1995 *Phys. Rev.* B **52** 3561
[6] Shishidou T, Oguchi T and Jo T 1999 *Phys. Rev.* B **59** 6813
[7] Yaouanc A, Dalmas de Réotier P, Sanchez J-P, Tschentscher T and Lejay P 1998 *Phys. Rev.* B **57** R681
Dunlap B D, Nowik I and Levy P M 1973 *Phys. Rev.* B **7** 4232
Berthier Y, Devine R A B and Belorizky E 1978 *Phys. Rev.* B **17** 4137
[8] Fournier J M and Tróc R 1985 *Handbook on the Physics and Chemistry of the Actinides* vol 2, ed A J Freeman and G H Lander (Amsterdam: North-Holland) p 105
[9] Wedgwood F A and Kuznietz M 1972 *J. Phys. C: Solid State Phys.* **5** 3012
[10] Buyers W J L and Holden T M 1985 *Handbook on the Physics and Chemistry of the Actinides* vol 2, ed A J Freeman and G H Lander (Amsterdam: North-Holland) p 239
[11] Wedgwood F A 1972 *J. Phys. C: Solid State Phys.* **5** 2427
[12] Reihl B, Erbudak M and Greuter F 1979 *J. Magn. Magn. Mater.* **13** 132
[13] Eib W, Erbudak M, Greuter F and Reihl B 1978 *Phys. Lett.* A **68** 391
Erbudak M and Meier F 1980 *Physica* B **102** 134
[14] Reim W and Schoenes J 1990 *Ferromagnetic Materials* vol 5, ed E P Wohlfarth and K H J Buschow (Amsterdam: North-Holland)

[15] Rogalev A, Goulon J, Sanchez J-P and Kernavanois N 1999 *European Synchrotron Radiation Facility Highlights* p 57
[16] Mannix D, Stunault A, Bernhoeft N, Paolasini L, Lander G H, Vettier C, de Bergevin F, Kaczorowski D and Czopnik A 2001 *Phys. Rev. Lett.* **86** 4128
[17] Demuynck S, Sandratskii L, Cottenier S, Meersschaut J and Rots M 2000 *J. Phys.: Condens. Matter* **12** 4629
[18] Lovesey S W and Collins S P (ed) 1996 *X-ray Scattering and Absorption by Magnetic Materials* (Oxford: Oxford Science)
[19] Collins S P, Laundy D, Tang C C and van der Laan G 1995 *J. Phys.: Condens. Matter* **7** 9325
[20] Cooper M J, Zukowski E, Collins S P, Timms N D, Itoh F and Sakurai H 1992 *J. Phys.: Condens. Matter* **4** L399
[21] Carra P, Fabrizio M and Thole B T 1996 *Phys. Rev.* B **53** R5994
[22] Lovesey S W 1996 *J. Phys.: Condens. Matter* **8** L353
[23] Lipps F W and Tolhoeck H A 1954 *Physica* **20** 85
Lipps F W and Tolhoeck H A 1954 *Physica* 395
[24] Honkimäki V, Private communication
McCarthy J 1997 *PhD Thesis* University of Warwick, Coventry
[25] Ribberfors R 1975 *Phys. Rev.* B **12** 2067
[26] Holm P 1988 *Phys. Rev.* A **37** 3706
[27] Kernavanois N 2000 *PhD Thesis* University of Grenoble
[28] Fajardo P, Honkimäki V, Buslaps Th and Suortti P 1998 *Nucl. Instrum. Methods* B **134** 337
[29] Tschentscher Th, McCarthy J E, Honkimäki V and Suortti P 1998 *J. Synchrotron Radiat.* **5** 940
[30] Sakurai H, Hashimoto H, Ochiai A, Suzuki T, Ito M and Itoh F 1995 *J. Phys.: Condens. Matter* **7** L599
[31] Hashimoto H, Sakurai H, Oike H, Itoh F, Ochiai A, Aoki H and Suzuki T 1998 *J. Phys.: Condens. Matter* **10** 6333
[32] Barbiellini B, Moroni E G and Jarlborg T 1990 *J. Phys.: Condens. Matter* **2** 7597
[33] Biggs F, Mendelsohn L B and Mann J B 1975 *At. Data Nucl. Data Tables* **16** 201
[34] Thole B T, Carra P, Sette F and van der Laan G 1992 *Phys. Rev. Lett.* **68** 1943
[35] Carra P, Thole B T, Altarelli M and Wang X 1993 *Phys. Rev. Lett.* **70** 694
[36] Dalmas de Réotier P, Sanchez J-P and Yaouanc A 1998 *J. Alloys Compounds* **271–273** 414
[37] Goulon J, Brookes N B, Gauthier C, Goedkoop J, Goulon-Ginet C, Hagelstein M and Rogalev A 1995 *Physica* B **208+209** 199
[38] Gauthier C, Goulon G, Feite S, Moguiline E, Braicovich L, Brookes N B and Goulon J 1995 *Physica* B **208+209** 232
[39] Malgrange C, Carvalho C, Braichovitch L and Goulon J 1991 *Nucl. Instrum. Methods* A **308** 390
[40] van Veenendaal M, Goedkoop J B and Thole B T 1996 *Phys. Rev. Lett.* **77** 1508
[41] Sparks C J 1980 *Synchrotron Radiation Research* ed H Winick and S Doniach (New York: Plenum) p 459
[42] Dalmas de Réotier P, Sanchez J-P, Yaouanc A, Finazzi M, Sainctavit Ph, Krill G, Kappler J-P, Goedkoop J, Goulon J, Goulon-Ginet C, Rogalev A and Vogt O 1997 *J. Phys.: Condens. Matter* **9** 3291
[43] Yaouanc A, Dalmas de Réotier P, van der Laan G, Hiess A, Goulon J, Neumann C, Lejay P and Sato N 1998 *Phys. Rev.* B **58** 8793
Dalmas de Réotier P, Yaouanc A, van der Laan G, Kernavanois N, Sanchez J-P, Smith J L, Hiess A, Huxley A and Rogalev A 1999 *Phys. Rev.* B **60** 10 606
[44] van der Laan G and Thole B T 1996 *Phys. Rev.* B **53** 14 458
[45] Busch G, Vogt O, Delapalme A and Lander G H 1979 *J. Phys. C: Solid State Phys.* **12** 1391
[46] Lander G H, Brooks M S S and Johansson B 1991 *Phys. Rev.* B **43** 13 672
[47] Hunter Dunn J, Arvanitis D, Carr R and Mårtensson N 2000 *Phys. Rev. Lett.* **84** 1031